Journal of Sound and Vibration (1998) **212**(1), 61–74

GROUND VIBRATIONS DUE TO A RECTANGULAR HARMONIC LOAD

D. V. Jones

University of the West of England, Department of Mathematical Sciences, Coldharbour Lane, Frenchay, Bristol BS16 1QY, England

D. Le Houedec

Ecole Centrale De Nantes, LMM, 1 Rue De La Noë, BP 92101 44321 Nantes Cedex 3, France

AND

M. Petyt

Institute of Sound and Vibration Research, University of Southampton, Highfield, Southampton, S017 1BJ, England

(*Received* 22 *July* 1997, *and in final form* 22 *October* 1997)

The transmission of vibrations in the vicinity of a rectangular harmonic vertical load, acting on a damped elastic layer overlying a damped elastic half-space of different material, is investigated theoretically, by using a semi-analytical approach. The solution involves a double Fourier transform with respect to two of the space variables of Navier's elastodynamic equations. The inverse double Fourier transform is achieved with the FFT algorithm. Results presented include transformed displacements in the wavenumber domain, actual displacements in the near field of the load, and the direct receptance at the load. Comparisons are made with results for a half-space and a layer over a rigid foundation, and with some experimental results.

1. INTRODUCTION

The original motivation for the work described in this paper was concern about vibrations caused by rail and road transport. Theoretical models which simulate the propagation of such vibration will be of use in optimizing the application of defensive measures such as trenches, or vibration absorbing material placed under either the source of vibration or a protected structure.

The ground is modelled as an hysteretically damped elastic layer overlying an hysteretically damped elastic half-space of different material, with an harmonic vertical load in the form of a rectangle. A rectangular load is more typical of those encountered in practice than the commonly used disc load. Equally, a flexible interface represents a closer approximation to reality than either a layer over a rigid foundation, or a simple half-space. The load boundary condition is defined as a force rather than a displacement, to avoid mixed boundary conditions. A double Fourier transform is used to find the transformed displacements in the wavenumber domain. Explicit expressions for the three components of transformed displacements are found as functions of the two transform variables, which are the wavenumbers in the two horizontal directions. The actual displacements are then found by using a numerical inverse Fourier transform.

0022–460X/98/160061 + 14 $25.00/0/sv971367

In most previous work involving three-dimensional modelling of the ground structure considered here, the load has been modelled as either a point or a disc, to maintain cylindrical symmetry; see references [1] and [2] for example. The simpler two-dimensional (plane) problem has been considered by, among others, Newlands [3] and Israil and Ahmad [4]. An interesting alternative ground structure caled Gibson soil, in which the shear modulus varies in proportion to the depth, was modelled by Awojobi [5].

2. FOURIER TRANSFORM OF THE GOVERNING EQUATIONS

The model of the ground, co-ordinate system and load are shown in Figure 1. The rectangle has sides of length $2b$ and $2c$, and is aligned with respect to the co-ordinate axes as shown. It rests on an homogeneous, isotropic layer, with material properties E (Young's modulus), ρ (density) and v (Poisson ratio), which overlies a half-space with corresponding properties E', ρ' and v'. Throughout, quantities in the half-space are denoted with a prime. The layer and the half-space exhibit hysteretic damping characterized by loss factors η and η', and as a result the constants E, λ and μ (see equations (2) and (3) for the definitions of λ and μ) are each multiplied by a factor $(1 + i\eta)$, and likewise the half-space parameters E', λ', and μ', are multiplied by $(1 + i\eta')$, causing these constants to become complex. An harmonic vertical load acts uniformly over the rectangle, and no shear stresses exist at the surface. The first part of the approach is similar to that in reference [6], and will be summarized.

The behaviour of the layer is described by Navier's elastodynamic equations (see reference [7] Appendix A, for example). In the absence of a body force, and assuming the motion is harmonic, one obtains the following vector equation for the displacement vector $\mathbf{u}$ in the layer, which has components (u, v, w):

$$(\lambda + \mu)\mathbf{V}\Delta + \mu\mathbf{V}^2\mathbf{u} + \rho\omega^2\mathbf{u} = \mathbf{0}, \tag{1}$$

in which λ and μ, the Lamé constants, are defined as

$$\lambda = \frac{vE(1 + i\eta)}{(1 + v)(1 - 2v)}, \qquad \mu = \frac{E(1 + i\eta)}{2(1 + v)}. \tag{2, 3}$$

Similar equations relate the primed constants (E', etc.) in the half-space. In equation (1) $\mathbf{V}$ is the gradient, $\mathbf{V}^2$ is the Laplacian operator, and Δ is the dilatation, defined by

$$\Delta = \partial u/\partial x + \partial v/\partial y + \partial w/\partial z. \tag{4}$$

Taking the divergence of equation (1) and dividing by ρ gives

$$(\mathbf{V}^2 + k_1^2)\Delta = 0, \tag{5}$$

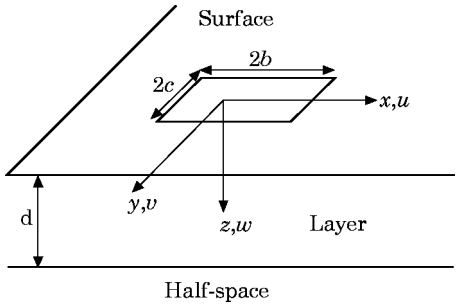

Figure 1. A diagram of the model.

where $k_1 = \omega/c_1$ and $c_1^2 = (\lambda + 2\mu)/\rho$. To solve equation (5), the double Fourier transform is used, which is defined as

$$\overline{f}(\beta, \gamma, z) = \int_{-\infty}^{\infty} \int_{-\infty}^{\infty} f(x, y, z)\, \mathrm{e}^{-\mathrm{i}(\beta x + \gamma y)}\, \mathrm{d}x\, \mathrm{d}y. \tag{6}$$

With the above definition of the Fourier transform, the corresponding inverse transform will include a factor $1/(4\pi^2)$. Applying the Fourier transform to equation (5) yields a simple differential equation for the transform of the dilatation, the solution of which is

$$\overline{\Delta} = A\, \mathrm{e}^{-\alpha_1 z} + B\, \mathrm{e}^{\alpha_1 z}, \tag{7}$$

where

$$\alpha_1^2 = \beta^2 + \gamma^2 - k_1^2. \tag{8}$$

Taking the Fourier transform of equation (1), substituting for $\overline{\Delta}$ and solving the resulting differential equation in z leads to

$$\begin{pmatrix} \bar{u} \\ \bar{v} \\ \bar{w} \end{pmatrix} = \begin{pmatrix} -\mathrm{i}\beta \\ -\mathrm{i}\gamma \\ \alpha_1 \end{pmatrix} \frac{A}{k_1^2}\, \mathrm{e}^{-\alpha_1 z} + \begin{pmatrix} -\mathrm{i}\beta \\ -\mathrm{i}\gamma \\ -\alpha_1 \end{pmatrix} \frac{B}{k_1^2}\, \mathrm{e}^{\alpha_1 z} + \begin{pmatrix} C \\ E \\ G \end{pmatrix} \mathrm{e}^{\alpha_2 z} + \begin{pmatrix} D \\ F \\ H \end{pmatrix} \mathrm{e}^{-\alpha_2 z}, \tag{9}$$

where $A, B, \ldots, H$ are functions of the wavenumbers β and γ, and

$$\alpha_2^2 = \beta^2 + \gamma^2 - k_2^2, \tag{10}$$

where $k_2 = \omega/c_2$ and $c_2^2 = \mu/\rho$. The constants G and H can be found in terms of the other unknowns by transforming the dilatation (equation (4)), substituting for the transformed displacements from equation (9), and equating the result to equation (7).

The stress–strain relations can be expressed as

$$\tau_{ij} = \lambda \delta_{ij}\, \Delta + \mu(\partial u_i / \partial x_j + \partial u_j / \partial x_i), \tag{11}$$

where τ_{ij} is the stress tensor, δ_{ij} is the Kronecker delta, and u_i and x_i are the ith components of the vectors (u, v, w) and (x, y, z) respectively. The stress components τ_{xz} and τ_{yz} are zero at the surface, while the component τ_{zz} at the surface can be written as

$$\tau_{zz|z=0} = \begin{Bmatrix} -P/4bc, & |x| < b, & |y| < c \\ 0, & \text{elsewhere} & \end{Bmatrix}. \tag{12}$$

P is the total force acting on the rectangle, and is equally distributed over it.

Using equation (9) to replace $\bar{u}$, $\bar{v}$ and $\bar{w}$ in the transform of equation (11), and evaluating the resulting expressions at $z = 0$, leads to the following three equations:

$$\frac{2\mathrm{i}\alpha_1 \beta}{k_1^2}(A - B) + \frac{(\beta^2 + \alpha_2^2)}{\alpha_2}(C - D) + \frac{\beta\gamma}{\alpha_2}(E - F) = 0, \tag{13}$$

$$\frac{2\mathrm{i}\alpha_1 \gamma}{k_1^2}(A - B) + \frac{\beta\gamma}{\alpha_2}(C - D) + \frac{(\gamma^2 + \alpha_2^2)}{\alpha_2}(E - F) = 0, \tag{14}$$

$$\left(\lambda - \frac{2\mu\alpha_1^2}{k_1^2}\right)(A + B) - 2\mu\mathrm{i}(\beta(C + D) + \gamma(E + F)) = -\frac{P \sin \beta b \sin \gamma c}{bc\beta\gamma}. \tag{15}$$

Because of possible over/underflow problems associated with terms of the form $\theta^{\pm\alpha z}$ for large z, sub-layers of depth h are introduced such that $d = nh$. The stiffness matrix for a sub-layer is then deduced and a global stiffness matrix for the entire physical layer constructed.

3. STIFFNESS MATRIX FOR A SUB-LAYER

From the preceding, one can find the 6×6 matrix $\mathbf{S}$ of coefficients such that

$$\bar{\boldsymbol{\tau}} = \mathbf{SK}, \tag{16}$$

where

$$\bar{\boldsymbol{\tau}} = (-\bar{\tau}_{zx}(0), -\bar{\tau}_{zy}(0), -\mathrm{i}\bar{\tau}_{zz}(0), \bar{\tau}_{zx}(h), \tau_{zy}(h), \mathrm{i}\bar{\tau}_{zz}(h))^{\mathrm{T}} \tag{17}$$

and

$$\mathbf{K} = (A \quad B \quad C \quad D \quad E \quad F)^{\mathrm{T}}. \tag{18}$$

The vector $\bar{\boldsymbol{\tau}}$ is defined as in equation (17) to make the stiffness matrix $\mathbf{C}$, which is defined below, symmetric. The transformed displacements at the top and bottom of a sub-layer can be expressed as

$$\bar{\mathbf{U}} = \mathbf{TK}, \tag{19}$$

where

$$\bar{\mathbf{U}} = (\bar{u}(0), \bar{v}(0), \mathrm{i}\bar{w}(0), \bar{u}(h), \bar{v}(h), \mathrm{i}\bar{w}(h))^{\mathrm{T}} \tag{20}$$

and $\mathbf{T}$ is the appropriate matrix of coefficients. Combining equations (16) and (19), and introducing the stiffness matrix $\mathbf{C}$ such that

$$\mathbf{C} = \mathbf{ST}^{-1}, \tag{21}$$

gives

$$\bar{\boldsymbol{\tau}} = \mathbf{C}\bar{\mathbf{U}}. \tag{22}$$

Equation (22) is for the first sub-layer of depth h; one can easily assemble a global equation for n layers. The form of this global equation is

$$\mathbf{C}_G\,\bar{\mathbf{U}}_G = \bar{\boldsymbol{\tau}}_G, \tag{23}$$

where, for the simple case $n = 2$,

$$\mathbf{C}_G = \begin{pmatrix} C_{11} & C_{12} & C_{13} & C_{14} & C_{15} & C_{16} & 0 & 0 & 0 \\ C_{21} & C_{22} & C_{23} & C_{24} & C_{25} & C_{26} & 0 & 0 & 0 \\ C_{31} & C_{32} & C_{33} & C_{34} & C_{35} & C_{36} & 0 & 0 & 0 \\ C_{41} & C_{42} & C_{43} & C_{44}+C_{11} & C_{45}+C_{12} & C_{46}+C_{13} & C_{14} & C_{15} & C_{16} \\ C_{51} & C_{52} & C_{53} & C_{54}+C_{21} & C_{55}+C_{22} & C_{56}+C_{23} & C_{24} & C_{25} & C_{26} \\ C_{61} & C_{62} & C_{63} & C_{64}+C_{31} & C_{65}+C_{32} & C_{66}+C_{33} & C_{34} & C_{35} & C_{36} \\ 0 & 0 & 0 & C_{41} & C_{42} & C_{43} & C_{44} & C_{45} & C_{46} \\ 0 & 0 & 0 & C_{51} & C_{52} & C_{53} & C_{54} & C_{55} & C_{56} \\ 0 & 0 & 0 & C_{61} & C_{62} & C_{63} & C_{64} & C_{65} & C_{66} \end{pmatrix}, \tag{24}$$

TABLE 1

Parameters for the layer and half-space

E (Young's modulus)	269 MN/m^2
E'	1076 MN/m^2
ρ (density)	1550 kg/m^3
ρ'	2000 kg/m^3
v (Poisson ratio)	0·257
v'	0·257
η (loss factor)	0·1
η'	0·1
P (total applied force)	1 N
d (layer depth)	7 m
b (rectangle dimension)	0·3 m
c (rectangle dimension)	0·3 m
f (frequency of excitation)	64 Hz

in which C_{ij} is the element of $\mathbf{C}$ in the ith row and jth column, and

$$\bar{\mathbf{U}}_G = (\bar{u}(0), \bar{v}(0), \mathrm{i}\bar{w}(0), \bar{u}(h), \bar{v}(h), \mathrm{i}\bar{w}(h), \bar{u}(d), \bar{v}(d), \mathrm{i}\bar{w}(d))^{\mathrm{T}},$$

$$\bar{\boldsymbol{\tau}}_G = (-\bar{\tau}_{zx}(0), -\bar{\tau}_{zy}(0), -\mathrm{i}\bar{\tau}_{zz}(0), 0, 0, 0, \bar{\tau}_{zx}(d), \bar{\tau}_{zy}(d), \mathrm{i}\bar{\tau}_{zz}(d))^{\mathrm{T}}.$$

The stresses at the layer/half-space interface are unknown, but they can be expressed in terms of the displacements at the interface, as described in the next section.

4. EXPRESSIONS FOR THE TRANSFORMED STRESSES AT THE INTERFACE

With the assumption of a perfect bond between the layer and half-space, the stresses and displacements at $z = d$ and $z' = 0$ must be identical: i.e.,

$$(\bar{u}(d), \bar{v}(d), \bar{w}(d))^{\mathrm{T}} = (\bar{u}'(0), \bar{v}'(0), \bar{w}'(0))^{\mathrm{T}}, \tag{24}$$

or, symbolically,

$$\bar{\mathbf{U}}(\mathrm{d}) = \bar{\mathbf{U}}'(0). \tag{25}$$

Likewise

$$(\bar{\tau}_{zx}(d), \bar{\tau}_{zy}(d), \mathrm{i}\bar{\tau}_{zz}(d))^{\mathrm{T}} = (\bar{\tau}'_{zx}(0), \bar{\tau}'_{zy}(0), \mathrm{i}\bar{\tau}'_{zz}(0))^{\mathrm{T}}, \tag{26}$$

or, symbolically,

$$\bar{\boldsymbol{\tau}}(d) = \bar{\boldsymbol{\tau}}'(0). \tag{27}$$

The stresses in the half-space can be expressed as [8]

$$\bar{\boldsymbol{\tau}}'(0) = \mathbf{M}\mathbf{K}', \tag{28}$$

where $\mathbf{K}' = (A', B', C')$ is a vector of unknown constants and

$$\mathbf{M} = \mu' \begin{pmatrix} 2\mathrm{i}\beta\alpha'_1/k'^2_1 & -(\beta^2 + \alpha'^2_2)/\alpha'_2 & \beta\gamma/\alpha'_2 \\ 2\mathrm{i}\gamma\alpha'_1/k'^2_1 & \beta\gamma/\alpha'_2 & -(\gamma^2 + \alpha'^2_2)/\alpha'_2 \\ \mathrm{i}(k'^2_2 - 2(\beta^2 + \gamma^2))/k'^2_1 & 2\beta & 2\gamma \end{pmatrix}. \tag{29}$$

The displacements in the half-space can also be defined in terms of the vector $\mathbf{K}'$; one can write

$$\bar{\mathbf{U}}'(0) = \bar{\mathbf{U}}(d) = \mathbf{N}\mathbf{K}', \tag{30}$$

in which

$$\mathbf{N} = \begin{pmatrix} -\mathrm{i}\beta/k_1'^2 & 1 & 0 \\ -\mathrm{i}\gamma/k_1'^2 & 0 & 1 \\ \mathrm{i}\alpha_1'/k_1'^2 & -\beta/\alpha_2' & -\gamma/\alpha_2' \end{pmatrix}. \tag{31}$$

Eliminating $\mathbf{K}'$ in equations (28) and (30) and using equation (27) gives

$$\bar{\boldsymbol{\tau}}(d) = \mathbf{M}\mathbf{N}^{-1}\bar{\mathbf{U}}(d). \tag{32}$$

The stresses at the interface can thus be replaced by zeros in equation (23), by subtracting the symmetric matrix ($\mathbf{M}\mathbf{N}^{-1}$) from the bottom right corner of the matrix $\mathbf{C}_G$.

5. RESULTS

The global stiffness matrix $\mathbf{C}_G$ is diagonally dominant, and so no numerical difficulties are encountered when solving equation (23) for the transformed displacements. The layer in the ground was divided into seven sub-layers, giving a square global stiffness matrix with 24 rows. The parameters given in Table 1 have been used to produce the figures shown. They correspond to a particular site named Clarborough, which was also used in references [6] and [8], so aiding comparison with the results of those articles. The half-space parameters have been chosen partly because they are physically realistic, and also so that $E'/E = 4$, which ensures results characteristic of this model, since for $E'/E > 10$ the model behaves like a layer over a rigid foundation. A square load has been preferred ($b = c = 0{\cdot}3$ m) to emphasize the symmetry of the transformed displacements. Except where stated otherwise, a relatively high frequency for ground vibration of 64 Hz has been used, because with the chosen ground parameters this allows the development of several propagating modes in the 7 m layer, which gives interesting behaviour in both domains.

The behaviour of the transformed displacements in the (β, γ) plane is in itself informative, but for brevity only two such surfaces are shown here. In Figure 2 is shown the amplitude of the component $\bar{w}$; only the positive quarter-plane is shown, because $\bar{w}$

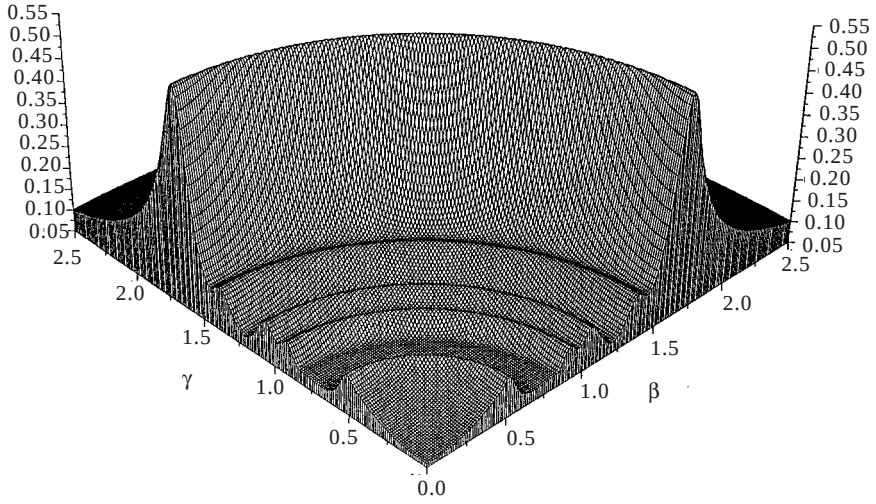

Figure 2. The amplitude of the transformed vertical displacement, $\bar{\omega}$. Vertical scale $\times 10^{-9}$.

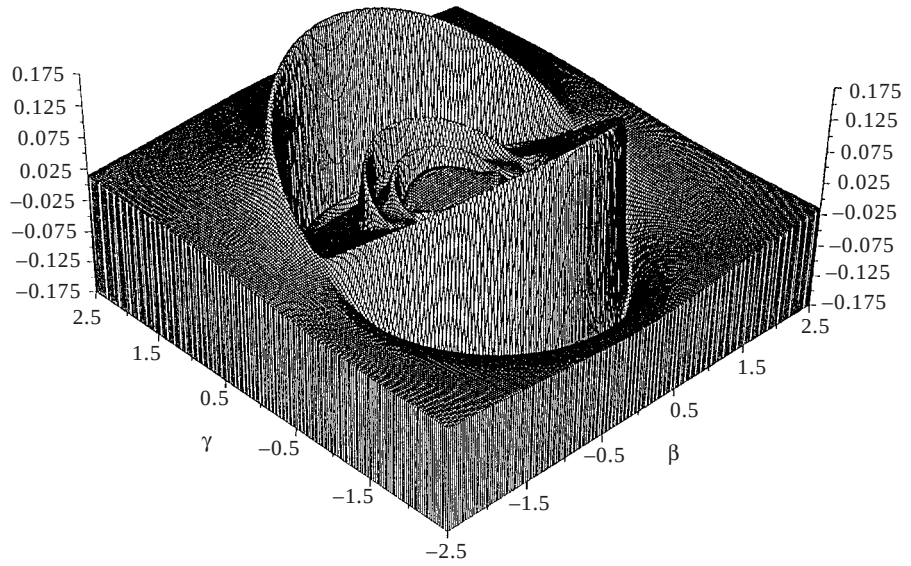

Figure 3. The imaginary part of the transformed transverse displacement, $\bar{v}$. Vertical scale $\times 10^{-9}$.

is symmetric with respect to both the $\beta = 0$ and $\gamma = 0$ planes. The peaks are located where the value of $(\beta^2 + \gamma^2)^{1/2}$ equals the wavenumber of one of the propagating modes in the layer (the approximate location of these peaks could be calculated using a free vibration analysis). The largest peak is located close to the wavenumber k_R of the Rayleigh wave (for zero damping and with the parameters used here, $k_R = 1{\cdot}67\ \mathrm{m}^{-1}$). This is because, for

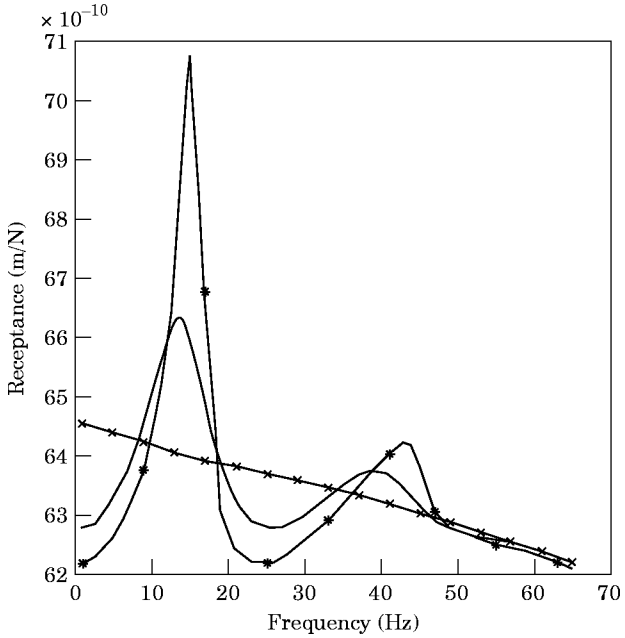

Figure 4. The modulus of the direct receptance. × × ×, Half-space; —, elastic foundation; ∗∗∗, inflexible, bedrock.

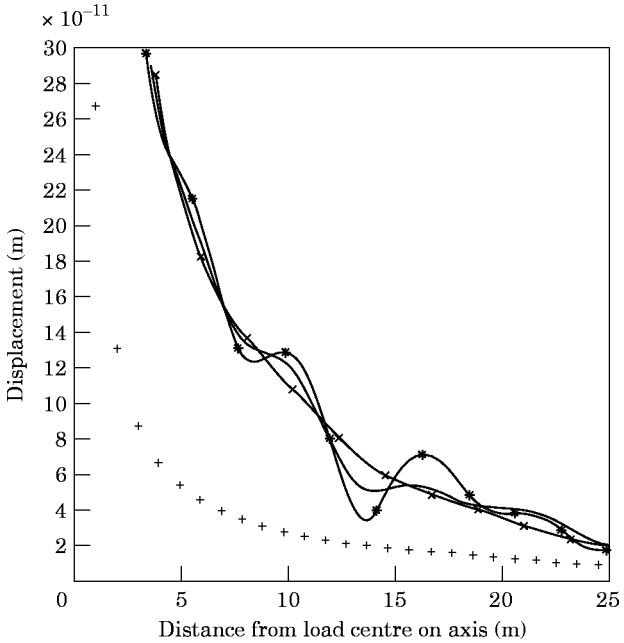

Figure 5. The amplitude of the vertical displacements along $x = 0$ for 64 Hz. Key as Figure 4, but with $+++$, no layer.

this combination of layer depth and frequency, the first mode is almost identical to the Rayleigh wave.

The imaginary part of the component $\bar{v}$ is shown in Figure 3. As in Figure 2, the locations of the peaks and troughs are related to the wavenumbers of the propagating modes in the layer. Both the real and imaginary parts of the component $\bar{v}$ are antisymmetric with respect to the β axis, and symmetric with respect to the γ-axis.

Under certain conditions, a generalized Rayleigh wave known as the Stoneley wave may exist at the interface. However, Scholte [9] has shown that Stoneley waves can exist only if the compression wave speeds in each medium are nearly equal, and likewise for the two shear wave speeds, which is not the case with the material properties used here.

The inverse transform was performed by using the Fast Fourier Transform (FFT) algorithm (see reference [10], for example), with a grid of 2048 points by 2048 and a range of $-16 < \beta, \gamma < 16$ to avoid aliasing and ensure an accurate representation of surfaces of the type shown in Figures 2 and 3.

In Figures 4 and 5 are shown results compared with those from models of a half-space [8], in which the layer material effectively extends to infinity, and a layer over an inflexible foundation [6], or "bedrock". In Figure 5 are also given displacements for a half-space of the material under the layer: that is, in which d shrinks to zero. In Figure 4 is shown the modulus of the direct receptance: i.e., the displacement per unit load P at the centre of the rectangular load for various frequencies. The data points have been joined by straight lines, which explains some discontinuities of gradient. The static responses for each model can be extrapolated from Figure 4 and, as expected, the simple half-space gives the greatest static receptance, while the present model gives a greater static displacement than the bedrock. The flexible interface used here can be seen as a compromise between the two extremes of a half-space and a bedrock; the strong resonance peaks associated with the bedrock are softened, because energy is now able to escape into the half-space below through coupling with the body waves; this can happen if the speed of a given mode

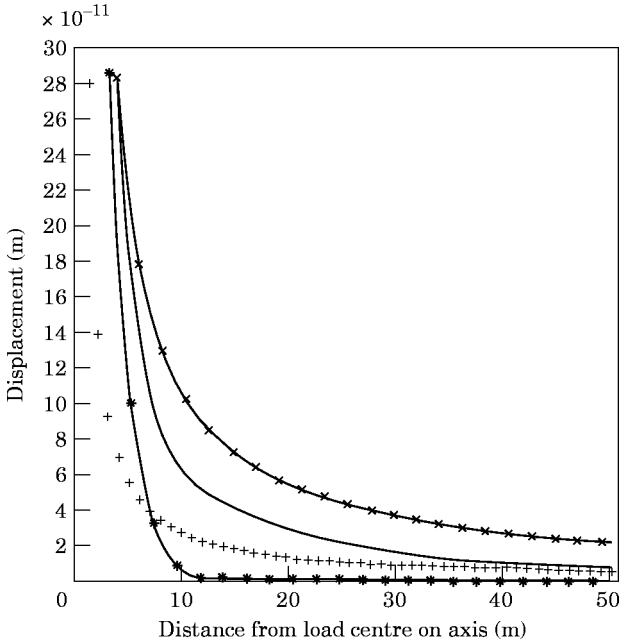

Figure 6. The amplitude of the vertical displacements along $x = 0$ for 10 Hz. Key as Figure 5.

exceeds the wave speed of the coupling body wave in the half-space [11]. The variation of both layer models from the half-space results is due to interference of the propagating modes. One can also note that for higher frequencies (above 50 Hz) the three receptances merge, because the wavelengths of the principal waves are too short for the interface to

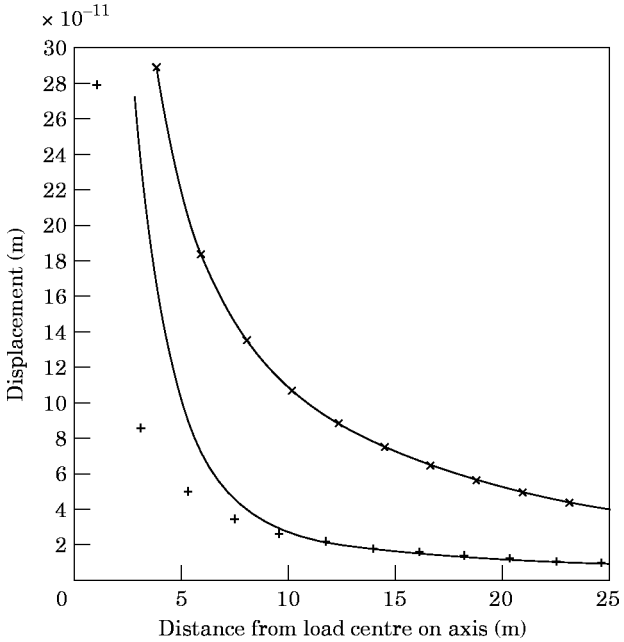

Figure 7. The amplitude of the vertical displacements along $x = 0$ for 4 Hz. Key as Figure 5.

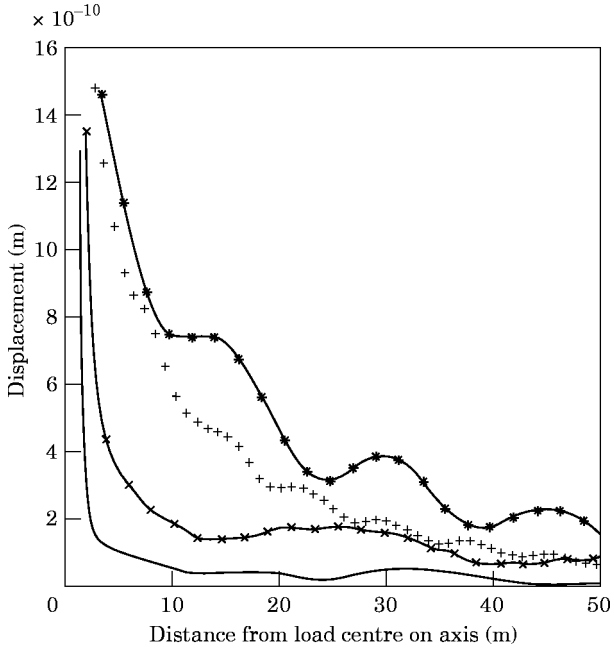

Figure 8. The results with the parameters in Table 2. Frequency (Hz): —, 16; × × ×, 32; ***, 44; + + +, 64.

have a significant effect (at 50 Hz with the parameters used here, the Rayleigh wavelength is less than 5 m, whereas the layer is 7 m deep).

In Figure 5 the three models up to 25 m from the load centre, along the x-axis, are compared. The displacements have been "clipped" to show the detail; the actual displacements at the load centre are all close to $6{\cdot}25 \times 10^{-9}$ m, with the exception of the "no layer" results (corresponding to $d = 0$), for which the displacement at the centre of the load is $1{\cdot}61 \times 10^{-9}$ m. Again, the elastic interface is a compromise between the other two models: the modes propagating over the elastic boundary produce a softer interference pattern than the bedrock model. The differences in the three displacements would be greater at the resonant frequencies, which can be deduced from Figure 4. The "no layer" results have been included to emphasize that, at 64 Hz, the behaviour is close to that for a layer extending to infinity, so that the half-space below has little effect on the displacements at the surface. Auersch [2] has stated the general rule that only the material to a depth of one half the Rayleigh wavelength λ_R has an effect on the surface displacements. At a frequency of 64 Hz, $\lambda_R = 3{\cdot}8$ m, and since $d = 7$ m the results in Figure 5 confirm Auersch's rule. To verify that this rule applies at lower frequencies, similar comparisons were undertaken for 10 Hz and 4 Hz, and are shown in Figures 6 and 7. At 10 Hz $\lambda_R = 24{\cdot}2$ m, so that more than two thirds of the Rayleigh wavelength extends into the half-space below the layer. More than 40 m from the load, it is clear that the response is very similar to that for $d = 0$ ("no layer"). However, within 5 m of the load, the material immediately below the load is decisive; the maximum response for the three models which include the layer material is close to $6{\cdot}6 \times 10^{-9}$ m, whereas the "no layer" model gives a corresponding displacement of $6{\cdot}3 \times 10^{-9}$ m. It may be noted that, at this low frequency, the "inflexible bedrock" model inhibits vibration propagation. For this reason, it has not been included in Figure 7, which is for 4 Hz, at which frequency $\lambda_R = 60$ m. In Figure 7 it is shown that, for a sufficiently low frequency, the layer material

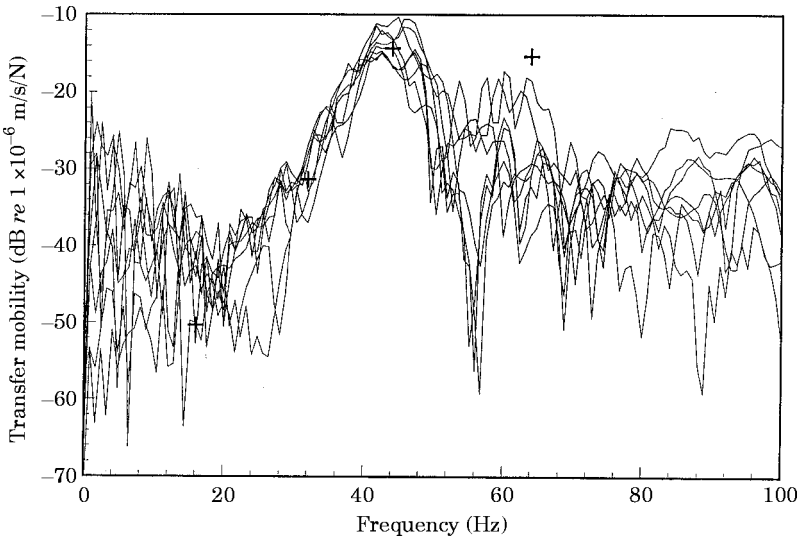

Figure 9. A comparison with the experimental data (vertical component).

only affects the surface response close to the load. At 10 m from the load and beyond, the response is practically identical to that for $d = 0$.

Figures 8, 9 and 10 have been included to allow a comparison with some experimental results [12]. In Figure 8 are shown vertical displacements up to 25 m from the load for four frequencies, and in Figures 9 and 10 the vertical and horizontal displacements, respectively, 15 m from the load, compared with the experimental data. For this comparison, the elastic foundation model had a layer depth of 1·98 m; the other parameters used are given in Table 2. They correspond to a site named Checkerhouse. The damping loss factor was proportional to frequency, as shown in the table. In Figure 8 it is shown that the displacements are sensitive to the distance from the load, because of the interference of the propagating modes in the layer. For example, at 44 Hz, a pronounced

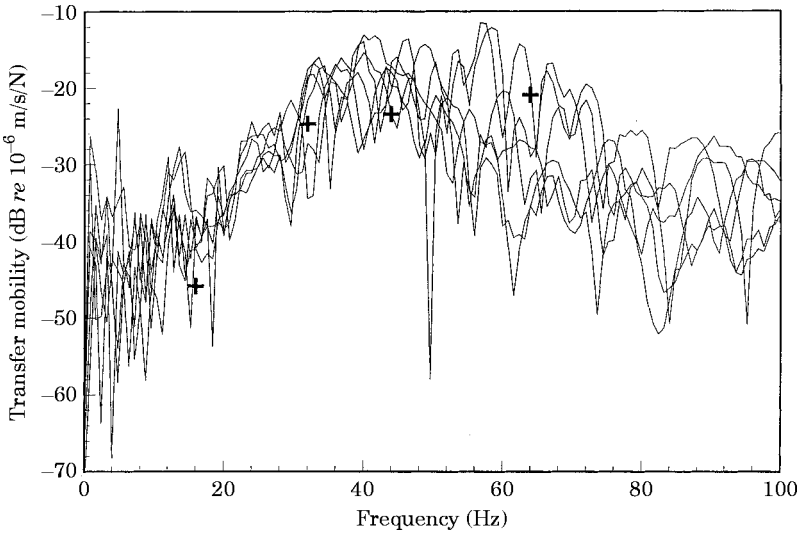

Figure 10. A comparison with the experimental data (horizontal component).

TABLE 2

Parameters for experimental comparison

E (Young's modulus)	157 MN/m^2
E'	1063 MN/m^2
ρ (density)	1517 kg/m^3
ρ'	1759 kg/m^3
v (Poisson ratio)	0·180
v'	0·253
η (loss factor)	0·00041 $\times f$
η'	0·00041 $\times f$
P (total applied force)	1 N
d (layer depth)	1·98 m
b (rectangle dimension)	0·177 m
c (rectangle dimension)	0·177 m

local minimum amplitude of displacement is found 24 m from the load. The experimental results were produced using a disc load of radius 10 cm, and so a square having the same surface area has been used as an approximation. The measured data are for transfer mobilities at 15 m from the load, given as dB *re* 10^{-6} m/s/N, and the matching vertical mobilities calculated with the present model at 15 m for the frequencies 16, 32, 44 and 64 Hz are, respectively, -50, -31, -14 and -15 dB. These compare well with the experimental data, as shown in Figure 9, in which the calculated values are shown with plus signs. The experimental results show a steep low frequency cut-off, with a maximum response near 44 Hz, and the results here follow this pattern. The corresponding calculated

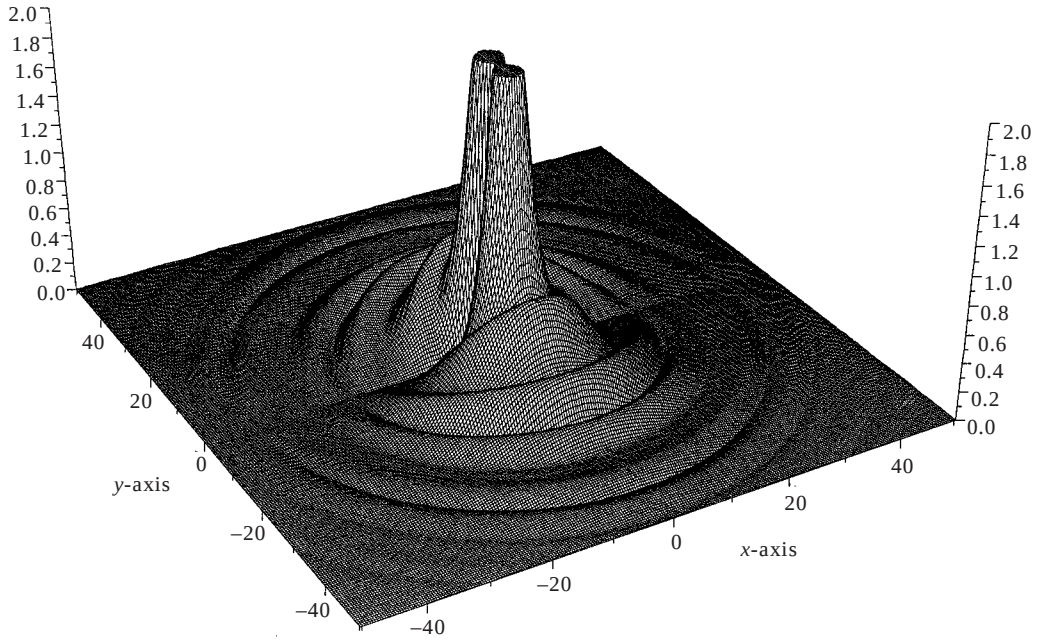

Figure 11. The amplitude of the vertical displacements (w) around the load. Vertical scale $\times 10^{-9}$; all scales in m.

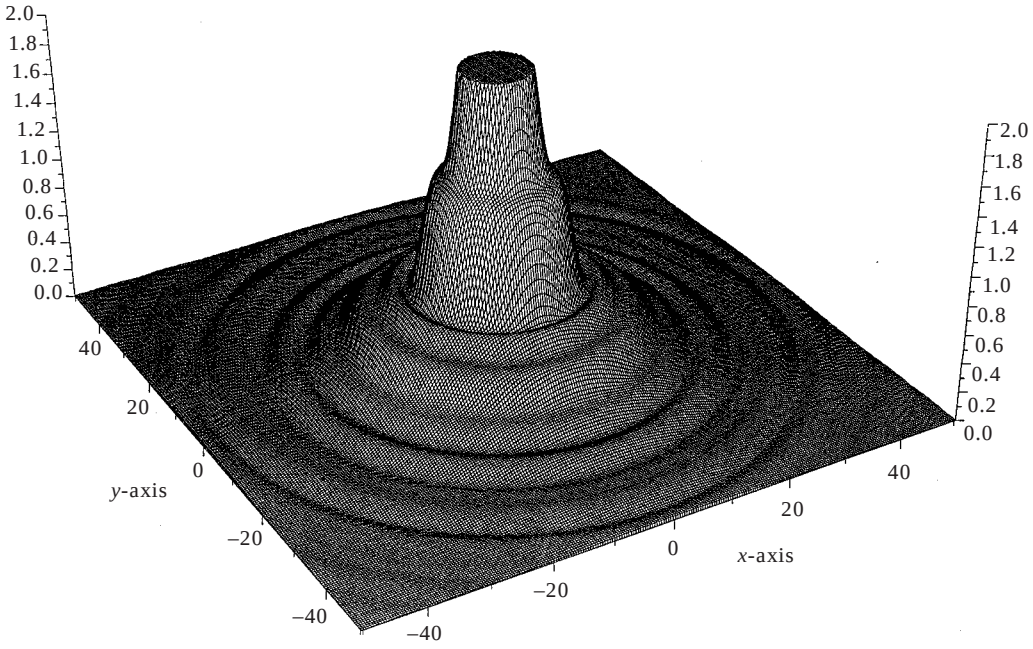

Figure 12. The amplitude of the transverse displacements (v) around the load. Scales as Figure 11.

horizontal mobilities are $-45{\cdot}6$, $-24{\cdot}3$, $-23{\cdot}0$ and $-20{\cdot}5$ dB, and in Figure 10 it is shown that these too compare well with the experimental data.

Finally, in Figures 11 and 12 are shown, respectively, vertical and transverse components of displacements (w and v) over the surface surrounding the load. The horizontal component u is not shown because, for a square load, this is identical to Figure 12 rotated through 90°. The displacements are clipped to show the detail; the actual maximum displacement in Figure 12, which occurs at the load edge, is $1{\cdot}07 \times 10^{-9}$ m. The vertical excitation produces a greater vertical than horizontal or transverse displacement at the surrounding surface, and the transverse component is zero along the line $y = 0$, as required physically.

6. CONCLUSIONS

A theoretical model of ground vibrations caused by an harmonic, vertical and rectangular load acting on a damped layer over a damped elastic half-space of different material has been developed. Results produced with the model have been compared with those for a simple half-space, and a damped elastic layer over a rigid foundation. The results presented show the form of the transformed displacements, the amplitudes of the components of actual surface displacments along the line $x = 0$, and also plotted as surfaces over the (x, y) plane, and the direct receptance of the rectangular load. Although the material in the layer always dictates the surface response close to the load, the response in the further field is dominated by the material in the half-space below for low frequencies, and by the layer material for high frequencies. The results compare well with published experimental work. Although results have been presented only for frequencies below 100 Hz, it may be remarked that the model could be applied to higher frequencies and thus to modelling ground-borne noise.

ACKNOWLEDGMENTS

D. V. Jones and D. Le Houédec acknowledge the support of the British Council and APAPE in France, for funding a travel grant which made much of this work possible.

REFERENCES

1. L. Girardi 1981 *Annales de l'ITBTP*, *Sols et Fondations* **397**, 31–66. Propagation des vibrations dan les sols homogènes ou stratifiés.
2. L. Auersch 1994 *Journal of Sound and Vibration* **173**, 233–264. Wave propagation in layered soils: theoretical solution in wavenumber domain and experimental results of hammer and railway traffic excitation.
3. M. Newlands 1952 *Philosophical Transactions of the Royal Society* **A245**, 896–897. The disturbance due to a line source in a semi-infinite elastic medium with a single surface layer.
4. A. S. M. Israil and S. Ahmad 1989 *Earthquake Engineering and Structural Dynamics* **18**, 933–950. Dynamic vertical compliance of strip foundations in layered soils.
5. A. O. Awojobi 1972 *Geotechnique* **22**, 333–343. Vertical vibrations of a rigid circular foundation on Gibson soil.
6. D. V. Jones, O. Laghrouche, D. Le Houedec and M. Petyt 1997 *Journal of Sound and Vibration* **203**, 307–319. Ground vibration in the vicinity of a rectangular load acting on a viscoelastic layer over a rigid foundation.
7. K. F. Graff 1975 *Wave Motion in Elastic Solids*. Oxford: Clarendon Press.
8. D. V. Jones and M. Petyt 1993 *journal of Sound and Vibration* **166**, 141–159. Ground vibration in the vicinity of a rectangular load on a half-space.
9. J. G. Scholte 1947 *Monthly Notices of the Royal Astronomical Society*, *Geophysical Supplement* **5**, 120–127. The range of existence of Rayleigh and Stoneley waves.
10. E. O. Brigham 1988 *The Fast Fourier Transform and its Applications*. Englewood Cliffs, N.J.: Prentice-Hall.
11. B. Stump 1984 *Journal of Sound and Vibration* **92**, 181–202. Stress waves in an elastic half-space: single and multiple surface sources.
12. A. T. Peplow, C. J. C. Jones and M. Petyt 1995 *Proceedings of the Institute of Acoustics Spring Conference* **17**(4), 479–486. Ground vibration over uniform and non-uniform layered media: a two dimensional model.